Effects of laminar burning velocity to friction velocity ratio on turbulent premixed flame-wall interaction within turbulent boundary layers

Umair Ahmed [1,*] Nilanjan Chakraborty [1] and Markus Klein [2]
[1]*School of Engineering, Newcastle University, Newcastle upon Tyne NE1 7RU, United Kingdom*
[2]*Department of Aerospace Engineering, University of the Bundeswehr Munich, Neubiberg, Germany*

(Received 8 April 2024; accepted 21 October 2024; published 18 November 2024)

Direct numerical simulation of flame-wall interaction (FWI) for two flame configurations under different laminar burning velocity to nonreacting wall friction velocity ratio, $S_L/u_{\tau_{\mathrm{NR}}}$, have been performed. The first configuration considered is a V-flame in a turbulent channel flow with isothermal inert walls and represents oblique wall interaction. The second configuration is representative of head-on interaction (HOI) of a planar flame interacting with a wall in a fully developed turbulent boundary layer. In the case of the V-flame with $S_L/u_{\tau_{\mathrm{NR}}} = 0.4$, a smaller flame angle is obtained when compared with that of the V-flame with $S_L/u_{\tau_{\mathrm{NR}}} = 0.7$. This is a consequence of the differences in the turbulent burning velocities between the two V-flame cases, where the case with $S_L/u_{\tau_{\mathrm{NR}}} = 0.4$ has a lower turbulent burning velocity when compared with that of the case with $S_L/u_{\tau_{\mathrm{NR}}} = 0.7$. By contrast, the ratio of turbulent to laminar burning velocity is higher for the $S_L/u_{\tau_{\mathrm{NR}}} = 0.4$ HOI case when compared to the corresponding HOI case with $S_L/u_{\tau_{\mathrm{NR}}} = 0.7$. The flame orientations with respect to the streamwise component of velocity and wall-normal direction in addition to the $S_L/u_{\tau_{\mathrm{NR}}}$ values have been found to have a significant impact on the variations of wall heat flux, wall shear stress, and wall friction velocity in premixed FWI within turbulent boundary layers. The behaviors of nondimensional streamwise velocity, u^+, and nondimensional temperature using wall units, T^+, have also been investigated for different $S_L/u_{\tau_{\mathrm{NR}}}$ ratios and it is found that the standard log-law profiles in the case of u^+ and T^+ are not valid for the two configurations and the two $S_L/u_{\tau_{\mathrm{NR}}}$ ratios considered.

DOI: 10.1103/PhysRevFluids.9.113201

I. INTRODUCTION

In the case of premixed flame-wall interaction (FWI) within turbulent boundary layers, the combustion process is strongly affected by the presence of walls [1]. Although extensive research has been directed to nonreacting turbulent boundary layers using Direct Numerical Simulations (DNS), these studies have relatively limited relevance to turbulent reacting flows within boundary layers due to thermal expansion effects arising from the combustion processes leading to significant modifications in the velocity and temperature distributions. The advances in high-performance computing have given rise to the possibility of analyzing FWI within turbulent boundary layers using DNS. The DNS of premixed FWI within turbulent boundary layer was pioneered by Alshaalan and Rutland [2] and Bruneaux *et al*. [3,4]. Alshaalan and Rutland [2] analyzed the performances of

*Contact author: umair.ahmed@newcastle.ac.uk

turbulent scalar flux and mean reaction rate closures during the interaction of a V-flame with an isothermal wall within a turbulent boundary layer. Bruneaux *et al*. [4] analyzed premixed turbulent FWI within turbulent channel flows for constant density conditions and used this data for the purpose of revising the Flame Surface Density (FSD)-based mean reaction rate closure for wall-bounded flows. Subsequently, several studies focused on the statistics of flame structure including species distributions [5–7], reacting scalar gradient [5,6,8], turbulent flow statistics including enstrophy, turbulent kinetic energy, and flame-vortex interactions [8–13], turbulent scalar flux, variance and dissipation rate statistics [12,14], wall heat transfer [11,15] and correlations of heat release rate and mixture fraction variation with flame curvature [16] during FWI within turbulent boundary layers.

One of the key independent nondimensional parameters for premixed flame-wall interaction is the ratio of laminar burning velocity to nonreacting flow wall friction velocity, $S_L/u_{\tau_{\mathrm{NR}}}$, which for a given channel flow configuration for a particular friction Reynolds number, Re_τ, can be modified by altering the mixture composition and the extent of preheating. This ratio can be considered as a measure of turbulence intensity to burning velocity ratio in FWI within turbulent boundary layers, which motivates the current analysis. In turbulent boundary layers, the root mean square (rms) velocity scales with $u_{\tau_{\mathrm{NR}}}$ and, thus, the inverse of this quantity plays the role of the ratio of the rms velocity to laminar burning velocity, which is a key parameter for the characterization of the premixed combustion process in Borghi-Peters diagram [17]. Despite the importance of $S_L/u_{\tau_{\mathrm{NR}}}$, only Bruneaux *et al.* [3] addressed the effects of $S_L/u_{\tau_{\mathrm{NR}}}$ and their analysis revealed that the $S_L/u_{\tau_{\mathrm{NR}}}$ can modify the turbulent burning velocity, wall heat flux magnitude, and wall normal variations of streamwise velocity and temperature within turbulent boundary layers during flame-wall interaction. However, the density change due to combustion was not accounted for by Bruneaux *et al*. [3] and an unsteady configuration where head-on quenching occurs was considered. The effects of $S_L/u_{\tau_{\mathrm{NR}}}$ on quasistationary flame-wall interaction have not been analyzed. It has been demonstrated by Ahmed *et al.* [9] that the relative alignment of the flame normal and wall normal direction affects the quenching distance, wall heat flux magnitude, and wall shear stress statistics during flame-wall interaction. Thus, in this paper, the effects of $S_L/u_{\tau_{\mathrm{NR}}}$ on turbulent burning velocity, wall heat flux magnitude, and wall-normal variations of streamwise velocity and temperature within turbulent boundary layers during flame-wall interaction have been analyzed by employing a variable density DNS of flame-wall interaction for both unsteady head-on quenching and statistically stationary oblique-wall quenching configurations.

In this paper, the turbulent flow statistics during FWI within turbulent boundary layers have been investigated under isothermal inert wall boundary conditions by performing DNS of oblique wall interaction (OWI) of a V-flame in a fully developed channel flow configuration and head-on interaction (HOI) of a statistically planar flame in a fully developed turbulent boundary layer. Two different values of $S_L/u_{\tau_{\mathrm{NR}}}$ have been investigated in the aforementioned configurations and $S_L/u_{\tau_{\mathrm{NR}}}$ values are set to below unity to avoid the possibility of boundary layer flashback.

The rest of the paper is organized as follows: In the next section, the description of the flow configurations and the details of the DNS data are provided, which is followed by the discussion of the results obtained from the analysis. Finally, the conclusions are drawn and main findings are summarized in the last section.

II. DIRECT NUMERICAL SIMULATION DATA

A three-dimensional (3D) fully compressible DNS code SENGA+ [18] has been used for carrying out the simulations of OWI of turbulent V-flames with isothermal inert walls in a turbulent channel flow configuration under different $S_L/u_{\tau_{\mathrm{NR}}}$ values. The same DNS code is used to simulate HOI of statistically planar flames with isothermal inert walls across fully developed turbulent boundary layers under different $S_L/u_{\tau_{\mathrm{NR}}}$ values. The governing equations for mass, momentum, energy, and species are solved in a nondimensional form. The code employs a tenth-order central difference scheme for the spatial discretisation, and the order of differentiation progressively reduces to a second-order scheme at the nonperiodic boundaries. A low storage third-order explicit Runge-Kutta

scheme is used for the time advancement of the solution. In all cases, a single-step Arrhenius-type chemical mechanism (fuel $+ s$ oxidizer $\rightarrow (1 + s)$products) representative of a methane-air mixture is employed for computational economy. Standard values are used for the Zeldovich number $\beta_z = T_a(T_{\rm ad} - T_R)/T_{\rm ad}^2 = 6.0$ (where T_a is the activation temperature, $T_{\rm ad}$ is the adiabatic flame temperature, and T_R is the temperature of the reactants), Prandtl number, $\Pr = 0.7$, and ratio of specific heats, $\gamma = 1.4$. The Lewis number, Le, of all the species is assumed to be unity and the heat release parameter, $\Gamma = (T_{\rm ad} - T_R)/T_R$ is set to 2.3. It has been demonstrated that the heat flux and quenching distance statistics obtained from simple chemistry DNS of FWI [2,6,19–21] are qualitatively and quantitatively similar to detailed chemistry DNS [22–26] and experimental [27–29] results. Furthermore, 1D HOI simulations at different wall temperatures, ranging from 300 K to 750 K, with a skeletal mechanism involving 16 species and 25 reactions proposed by Smooke and Giovangigli [30] have revealed that the variation in the dilatation rate during FWI remains almost within 3%–5% of the dilatation rate obtained from the single-step chemical reaction treatment. As the present analysis focuses primarily on turbulent flow and heat flux statistics, it is expected that the simplification of chemistry is unlikely to influence the conclusions of the current analysis.

The initial turbulence conditions for both flow configurations and inflow conditions for the V-flame simulation are obtained by performing an auxiliary DNS of an inert fully developed turbulent-plane channel flow driven by a streamwise constant pressure gradient. An overall momentum balance can be used to show that the pressure gradient is directly related to the shear stress as $-\partial p/\partial x = \rho u_{\tau_{\rm NR}}^2/h$, where $u_{\tau_{\rm NR}} = \sqrt{|\tau_{w_{\rm NR}}|/\rho_{\rm NR}}$ is the friction velocity for nonreacting channel flow (shown by the subscript NR), $\tau_w = \mu \partial u/\partial y|_{y=0}$ is the wall shear stress, h is the channel half height, and p is the pressure. The bulk Reynolds number $\mathrm{Re}_b = \rho u_b 2h/\mu$ for this simulation is 3285, where $u_b = 1/2h \int_0^{2h} u\, dy$, and the wall friction based Reynolds number $\mathrm{Re}_\tau = \rho u_\tau h/\mu$ is 110. The current grid spacing ensures that the minimum nondimensional distance of the grid points adjacent to the wall $y^+ = \rho_w u_\tau y/\mu_w$ is equal to 0.6, where y is the distance from the wall and subscript, w is used for wall quantities, and is at most $y^+ = 0.6$, which ensures appropriate resolution of the viscous sublayer. The validation of the nonreacting channel flow has been presented in Ref. [6] and is not repeated here. Two different values for $S_L/u_{\tau_{\rm NR}} = 0.7$ and 0.4 have been used in the current simulations.

The V-flame simulations are performed by placing a flame holder in the fully developed channel flow at $y^+ = 55$ from the bottom wall (i.e., $y = 0.5h$) with an approximate radius of $R_{f\rm th} \approx 0.2\delta_{\rm th}$ ($\delta_{\rm th} = (T_{\rm ad} - T_R)/\max|\nabla T|_L$, where the subscript L represents the laminar flame quantities) and the center positioned at $0.83h$ from the inlet of the channel. This location for the flame holder ensures that the flame interacts with the bottom wall at a reasonable distance and the viscous boundary layer is not influenced by the flame holder. The flame holder is defined following the definition used by Dunstan *et al.* [31] and the species, temperature and velocity distributions are imposed using a presumed Gaussian function defined as $g(r)A\exp[-r^2/2\xi^2]$, where A and ξ are adjustable constants to obtain the desired flame holder radius (i.e., $r = 0.2\delta_{\rm th}$ in this case). The source/sink terms in the momentum and species mass fractions are given as $S_m = g(r)(u_i - u_{i0})$ and $S_s = g(r)(y_\alpha - Y_{\alpha P})$ for $\alpha = 1, N - 1$ where $Y_{\alpha P}$ is the burned gas value of the species mass fraction at equilibrium and u_{i0} is the initial mean velocity in the ith direction. According to this implementation, the flame holder can be interpreted to represent a catalytic wire aligned in the periodic direction, but this formulation is not designed to create the wake behind an actual flame holder. Thus, this formulation of the flame holder is motivated by the stabilization of the flame in the least numerically intrusive manner. Further details on the implementation of the flame holder for this simulation are available in Ref. [31]. The velocity fluctuations introduced at the inflow of the reacting channel are obtained by temporal sampling of the *temporally evolving turbulence* at a fixed streamwise location of the auxiliary nonreacting channel flow simulation. The time step chosen for the nonreacting simulation, while the data is being sampled, is the same as that of the reacting flow simulation. Note that two different domain sizes in the streamwise direction have been used for the V-flame simulations. A

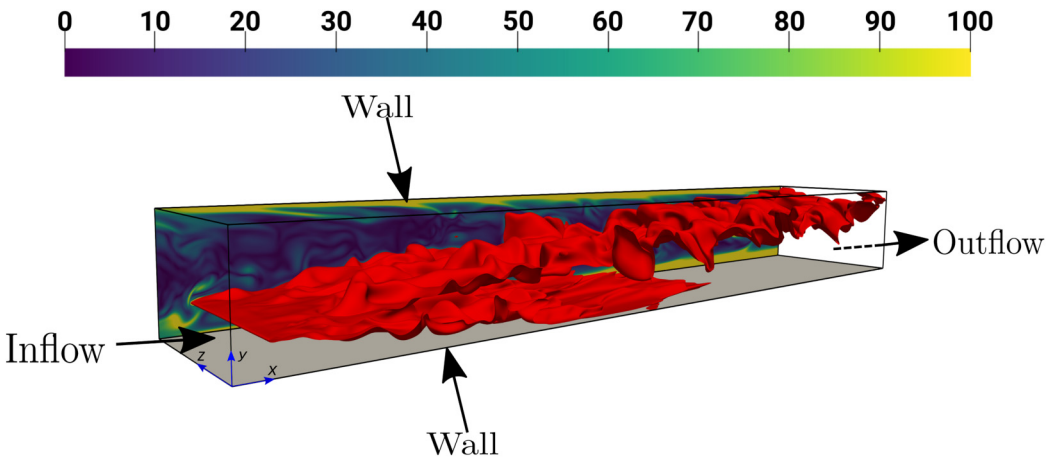

FIG. 1. V-flame with $S_L/u_{\tau_{\mathrm{NR}}} = 0.4$. The isosurface colored in red represents $c = 0.5$. The instantaneous normalized vorticity magnitude $\mathbf{\Omega}$ is shown on the x-y plane. The grey surface denotes the bottom wall.

domain size of $10.69h \times 2h \times 4h$, discretized on $1920 \times 360 \times 720$ equidistant grid points, is used for the $S_L/u_{\tau_{\mathrm{NR}}} = 0.7$ case, while the $S_L/u_{\tau_{\mathrm{NR}}} = 0.4$ case has been simulated using $22.28h \times 2h \times 4h$, discretized on $4000 \times 360 \times 720$ equidistant grid points. The reason for choosing different domain sizes in the streamwise direction is because the location of FWI is modified by the variation in $S_L/u_{\tau_{\mathrm{NR}}}$, which will be demonstrated later in the paper.

The simulation setup for the V-flame is exemplarily shown in Fig. 1. The boundaries in the x direction are taken to be turbulent inflow with specified density and velocity components at $x = 0$ and partially nonreflecting outflow at $x = 10.69h$ for $S_L/u_{\tau_{\mathrm{NR}}} = 0.7$ case and $x = 22.28h$ for the $S_L/u_{\tau_{\mathrm{NR}}} = 0.4$ case. The outflow is specified using Navier-Stokes characteristic boundary conditions (NSCBC). No slip conditions are imposed for velocity at the walls (i.e., $y = 0$ and $y = 2h$), while the temperature boundary condition is specified using Dirichelet (i.e., $T_w = T_R$) conditions for isothermal walls. The boundaries in the z direction are treated as periodic. The background channel flow is considered unaltered while the thermochemistry of the flame is modified to bring about the changes in S_L and δ_{th} but the unburned gas density, viscosity, specific heat, temperature, and γ are kept unaltered. The laminar flame thermal thickness δ_{th} for the $S_L/u_{\tau_{\mathrm{NR}}} = 0.7$ case is resolved using approximately eight grid points, while this increases to 16 for the $S_L/u_{\tau_{\mathrm{NR}}} = 0.4$ case. The simulations have been performed for approximately three flow-through times and the data has been sampled after one flow-through time once the initial transience has decayed. Note that under the current flow conditions, one flow-through time is enough to obtain a statistically stationary solution for the mean turbulent kinetic energy statistics. The instantaneous flame structures represented by the $c = (Y_{F_R} - Y_F)/(Y_{F_R} - Y_{F_P}) = 0.5$ (where Y_F is the fuel mass fraction and the subscripts R and P represent the respective values of the fuel in the unburned and fully burned gases) isosurface along with the normalized vorticity magnitude $\mathbf{\Omega} = \sqrt{\omega_i \omega_i} \times h/u_\tau$ (where ω_i is the ith component of vorticity) are shown in Fig. 1 for the $S_L/u_{\tau_{\mathrm{NR}}} = 0.7$ case.

The planar flame simulation in a turbulent boundary layer is performed by taking the solution from the fully developed turbulent channel flow up to $y/h = 1.33$ over the entire x-z plane. The domain size for this configuration is taken to be $10.69h \times 1.33h \times 4h$, which is discretized on $1920 \times 240 \times 720$ equidistant grid points for both $S_L/u_{\tau_{\mathrm{NR}}}$ values. The schematic of the flow configuration is presented in Fig. 2. The boundary conditions for this case are imposed as periodic in the x and z directions and a mean streamwise pressure gradient is applied in the x direction to drive the flow. The boundaries in the y direction are treated as the wall at $y = 0$ where a no-slip condition is imposed for velocity, while the temperature boundary condition at the wall is specified using the

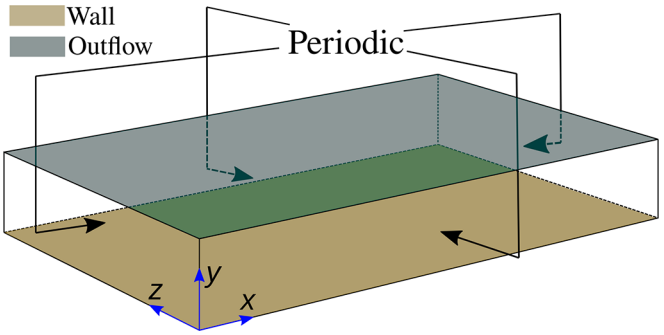

FIG. 2. Schematic of the computational domain used for head-on interaction of the statistically planar flame across a turbulent boundary layer.

same conditions as in the V-flame cases. An outflow boundary condition is specified at $y = 1.33h$ using NSCBC. This configuration is similar to the earlier work of Bruneaux *et al.* [3,4] in a constant density turbulent channel flow. The main difference is that in this case the density changes due to temperature rise and an outflow boundary is used to avoid any unnecessary thermodynamic pressure rise as a result of density variation due to combustion.

An unstretched laminar flame solution from a prior 1D flame simulation is interpolated onto the 3D grid and specified in a manner that $c = 0.5$ is centered at $y/h \approx 0.85$. The initial flame is specified such that the reactant side of the flame is facing the wall, while the product side of the flame is facing the outflow boundary in the y direction. The choice of the initial flame location and the length of the domain in the y direction is made based on the fact that the flame must remain sufficiently away from the outflow boundary at all times, while giving the flame enough time to wrinkle before interacting with the wall to obtain meaningful FWI statistics for a turbulent premixed flame. The resolution of the flame structure is identical to the V-flame case. During the simulation the flame propagates into the reactants and moves towards the wall, consequently interacting with the wall and quenching due to heat loss at the wall. In the case of $\mathrm{Re}_\tau = 110$, the root-mean-square velocity u' and longitudinal integral length scale, L_{11}, scale as $u_{\tau_{\mathrm{NR}}}$ and h [32], respectively, which indicates Damköhler and Karlovitz numbers of $\mathrm{Da} = L_{11}S_L/(u'\delta_{th}) = 5.83(15.80)$ and $Ka = (u'/S_L)^{3/2}(L_{11}/\delta_{\mathrm{th}})^{-1/2} = 1.01(0.36)$, respectively, for $S_L/u_{\tau_{\mathrm{NR}}} = 0.4(0.7)$. These values are representative of the flamelets combustion regime [17] away from the wall.

During the postprocessing of this configuration, the Reynolds-averaged quantities, Favre-averaged quantities, correlations involving Reynolds fluctuations and Favre fluctuations have been evaluated by spatial averaging in the periodic (x and z) directions for each snapshot. The results are reported in terms of the normalized simulation time t/t_f, where t_f is the chemical timescale. In these simulations, t/t_f is representative of the mean flame location in the y direction at a given snapshot. Figure 3 shows the time evolution of the flame-boundary layer interaction at different time instants in the simulation with $S_L/u_{\tau_{\mathrm{NR}}} = 0.4$ and the corresponding figures for the $S_L/u_{\tau\mathrm{NR}} = 0.7$ case are shown elsewhere [6,9,10,14] and thus are not repeated here. The instantaneous flame structures are represented by the $c = 0.5$ isosurface along with the normalized vorticity magnitude $\mathbf{\Omega}$. The vorticity generated in the vicinity of the wall within the turbulent boundary layer can also be seen in Fig. 3 and these vortical structures can play a key role in the FWI and more discussion on this can be found elsewhere [6,9,10,14,33]. It should be recognized here that the bulk and friction Reynolds numbers for the simulations performed in this paper are comparable to the recent state-of-the-art experiments performed for FWI [34] and these conditions are representative of flows found in IC engines. Recently, it has been demonstrated by Ahmed *et al.* [35,36] and Kai *et al.* [8] that the statistics presented in this paper do not change qualitatively with the variation in Re_τ.

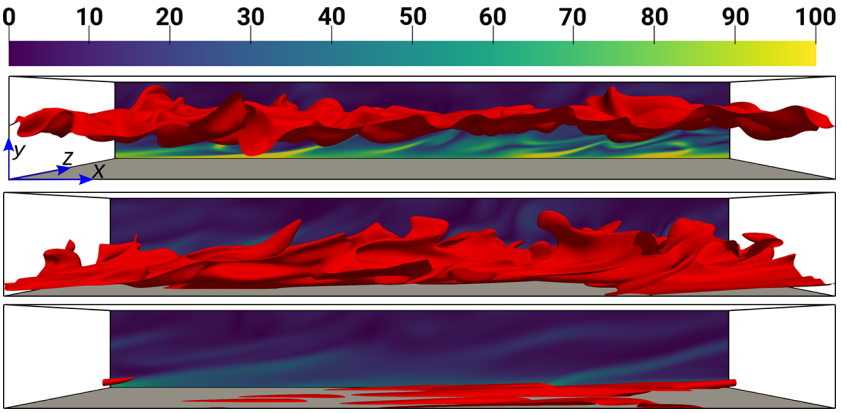

FIG. 3. Head-on interaction of statistically planar flame for $S_L/u_{\tau_{\mathrm{NR}}} = 0.4$ at different time instants. From top to bottom $t/t_f = 1.71$, $t/t_f = 5.48$, $t/t_f = 7.89$. The isosurface colored in red represents $c = 0.5$. The instantaneous normalized vorticity magnitude $\mathbf{\Omega}$ is shown on the x-y plane.

III. RESULTS AND DISCUSSION

Figure 4 shows the distribution of Favre mean progress variable for the V-flame cases. It can be seen from Fig. 4 that the flame interacts with the wall downstream of the flame holder and the flame brush thickness increases at the wall. This behavior is consistent with the earlier findings of Gruber *et al.* [5] and Alshaalan and Rutland [2] in the case of isothermal walls. It is visible from Fig. 4 that the flame interacts with the wall at a distance closer to the flame holder in the $S_L/u_{\tau_{\mathrm{NR}}} = 0.7$ case than in the $S_L/u_{\tau_{\mathrm{NR}}} = 0.4$ case. The distribution of $\widetilde{c}$ in the case of the planar flame HOI is presented in Fig. 5, which shows the thickening of the mean flame brush due to the interaction with the turbulence within the boundary layer. In the case of HOI, the flame propagates towards the wall as time progresses before interacting with the wall and eventually quenching due to heat loss at the wall. Note that similar to the V-flame cases, the planar flame HOI case with $S_L/u_{\tau_{\mathrm{NR}}} = 0.4$ shows different $\widetilde{c}$ profiles when compared with the corresponding $S_L/u_{\tau_{\mathrm{NR}}} = 0.7$ case. It can be seen from

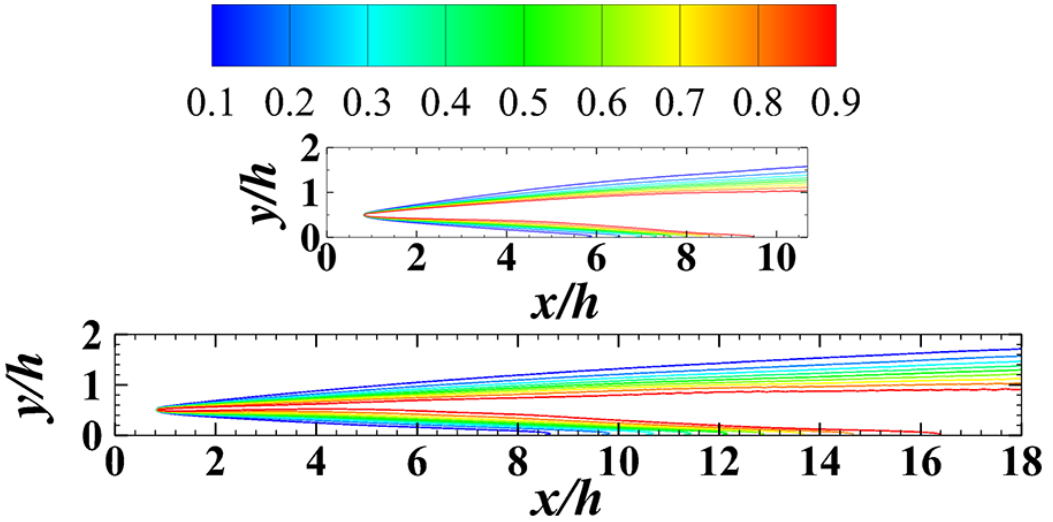

FIG. 4. $\widetilde{c}$ contours for the V-flame with $S_L/u_{\tau_{\mathrm{NR}}} = 0.7$ (top) and 0.4 (bottom).

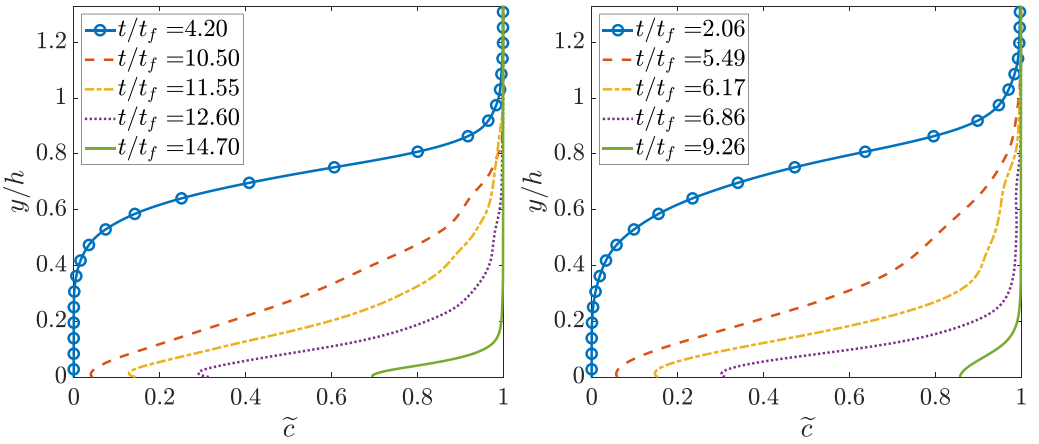

FIG. 5. $\widetilde{c}$ profiles for the planar flame at different time instants with $S_L/u_{\tau_{\rm NR}} = 0.7$ (left) and 0.4 (right).

Fig. 5 that in the $S_L/u_{\tau_{\rm NR}} = 0.4$ case, the flame interacts with the wall at a smaller value of t/t_f. This is in contrast to the behavior of the V-flame case with $S_L/u_{\tau_{\rm NR}} = 0.4$, where the flame has a much narrower angle when compared with the corresponding $S_L/u_{\tau_{\rm NR}} = 0.7$ case. The reasons for this variation are discussed in detail later on in the paper.

Figure 6 shows the behaviors of the mean profiles of density, temperature, reaction progress variable, and fuel mass fraction for the V-flame cases in the regions of FWI for the two $S_L/u_{\tau_{\rm NR}}$ ratios considered. The difference between $\widetilde{c}$ and $\widetilde{T}$ (where $T = (\hat{T} - T_R)/(T_{\rm ad} - T_R)$ is the nondimensional temperature and $\hat{T}$ is the local dimensional temperature) in the near wall region can be seen in both cases. The behavior of $\widetilde{c}$ and $\widetilde{T}$ in the case of isothermal wall boundary conditions is consistent with the earlier DNS of Gruber *et al.* [5] and Alshaalan and Rutland [2] involving V-flame simulations and also with the experimental findings of Jainski *et al.* [37]. In the case of planar flame HOI simulations the behaviors of the mean profiles of density, temperature, reaction progress variable and fuel mass fraction are presented in Fig. 7. At earlier times, there is no interaction of the flame with the wall, hence the profiles for $\widetilde{T}$ and $\widetilde{c}$ are identical to each other under both $S_L/u_{\tau_{\rm NR}}$ conditions. However, at later times (i.e., $t/t_f > 10.0$ in the case of $S_L/u_{\tau_{\rm NR}} = 0.7$ and $t/t_f > 5.0$ for $S_L/u_{\tau_{\rm NR}} = 0.4$) $\widetilde{T} \neq \widetilde{c}$ is obtained due to FWI.

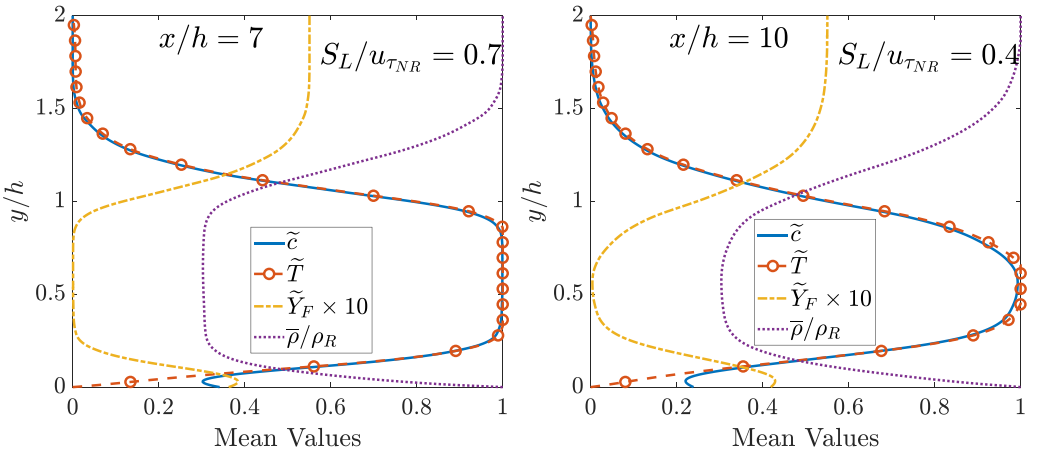

FIG. 6. Profiles for $\widetilde{c}$, $\widetilde{T}$, $\overline{\rho}/\rho_R$, and $\widetilde{Y}_F \times 10$ in the V-flame at $x/h = 7$ with $S_L/u_{\tau_{\rm NR}} = 0.7$ and 0.4.

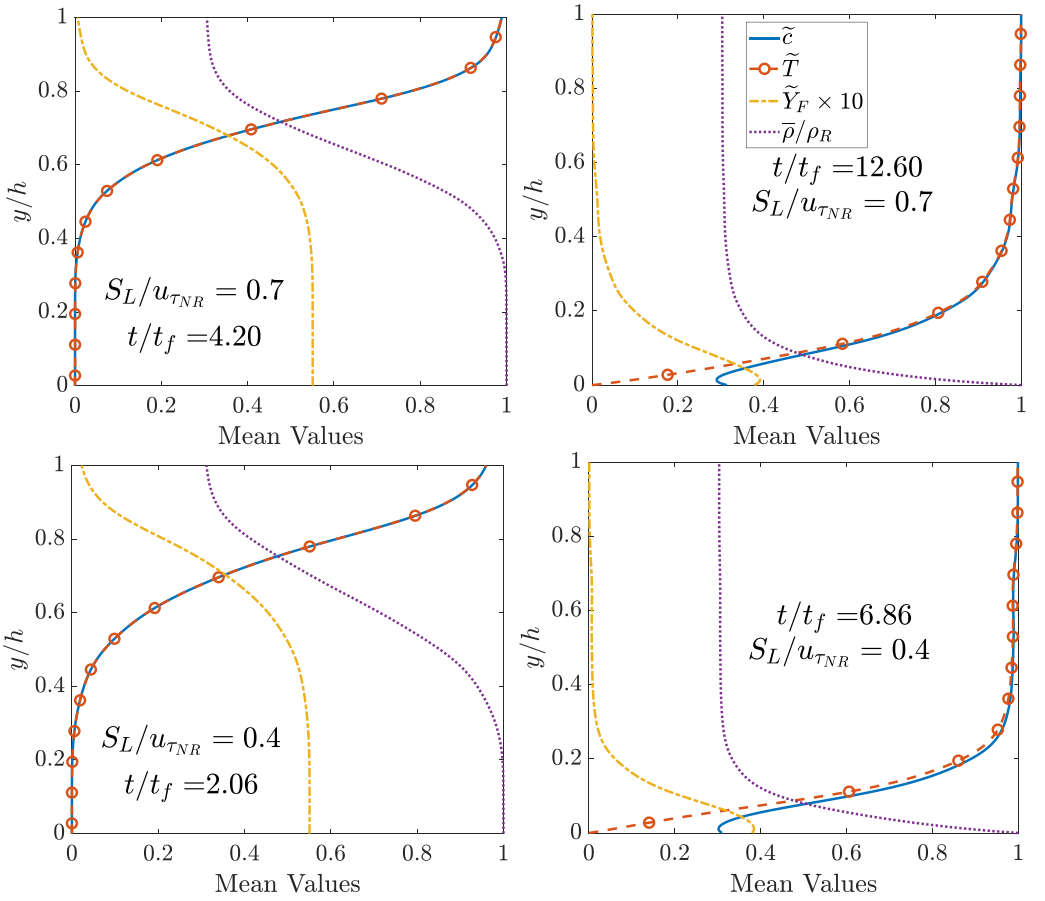

FIG. 7. Profiles for $\widetilde{c}$, $\widetilde{T}$, $\overline{\rho}/\rho_R$, and $\widetilde{Y}_F \times 10$ in the planar flame HOI cases at different time instants with $S_L/u_{\tau_{\mathrm{NR}}} = 0.7$ and 0.4 conditions.

Note that the intersection point of the V-flame with the wall in the x direction is determined by the turbulent burning velocity $S_T = (1/(\rho_R A_p)) \int_V \dot{w}_c dV$ as well as the bulk mean velocity, and the latter is unaltered in both cases. Here ρ_R is the density in the reactants, A_p is the projected flame area, and $\dot{w}_c$ is the reaction rate of the progress variable. In the V-flame cases, A_p is evaluated based on the angle of the $\widetilde{c} = 0.5$ isoline. In the case of V-flame simulations, S_T/S_L has been evaluated in the region of FWI, x/h between 6 and 9 for the $S_L/u_{\tau_{\mathrm{NR}}} = 0.7$ case while x/h between 8 and 16 is used for the $S_L/u_{\tau_{\mathrm{NR}}} = 0.4$ case. The resulting values for S_T/S_L are presented in Table I. The corresponding values for the flame area, $A_T = \int_V |\nabla c| dV$, normalized by A_p, are also presented in Table I for comparison. It can be noticed from Table I that the value of $S_T/S_L < 1$, which is expected

TABLE I. Values for S_T/S_L and A_T/A_p in the region of FWI for the V-flame cases with $S_L/u_{\tau_{\mathrm{NR}}} = 0.7$ and 0.4.

Case	S_T/S_L	A_T/A_p
$S_L/u_{\tau_{\mathrm{NR}}} = 0.7$	0.704	0.78
$S_L/u_{\tau_{\mathrm{NR}}} = 0.4$	0.519	0.55

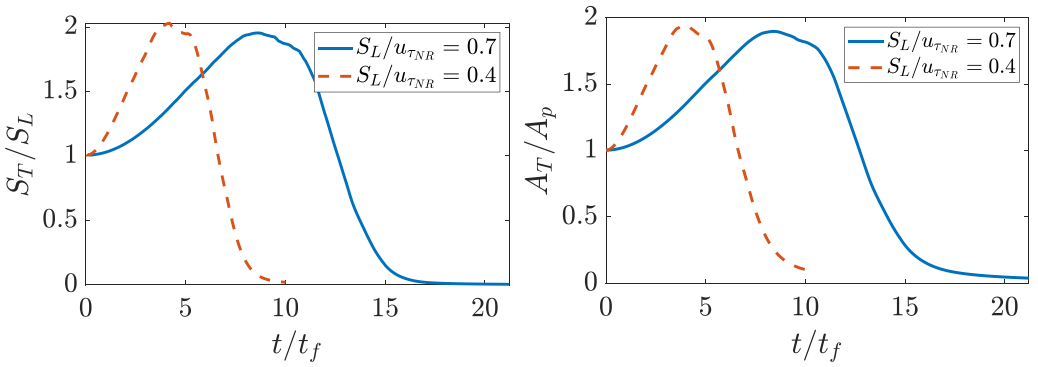

FIG. 8. Profiles for S_T/S_L (left) and A_T/A_p (right) in the planar flame HOI cases with $S_L/u_{\tau_{\mathrm{NR}}} = 0.7$ and 0.4.

in this region, as the flame starts to quench in this zone and S_T values tend to reduce. A similar trend to that of S_T/S_L is observed for A_T/A_p in this region for both V-flame cases. It is important to note that the overall values of S_T/S_L remain smaller for the V-flame with $S_L/u_{\tau_{\mathrm{NR}}} = 0.4$ than in the $S_L/u_{\tau_{\mathrm{NR}}} = 0.7$ V-flame case. Note that a higher value of S_T/S_L yields a larger flame angle, so it interacts with the wall at a smaller streamwise distance downstream of the flame holder. As the nonreacting turbulence is the same for both S_L/u_τ ratios the ratio of the longitudinal integral length scale in the streamwise direction to δ_{th} is smaller in the case of $S_L/u_{\tau_{\mathrm{NR}}} = 0.4$ than for the $S_L/u_{\tau_{\mathrm{NR}}} = 0.7$ case, because the flame thickness scales with D_c/S_L and the diffusivity, D_c, remains constant for both cases (i.e., δ_{th} is larger for $S_L/u_{\tau_{\mathrm{NR}}} = 0.4$). It should be recognized that the mean direction of flame propagation has a significant component in the streamwise direction in the V-flame configuration and has been demonstrated in previous analyses [38,39] that S_T/S_L decreases with a decrease in the ratio of the longitudinal integral length scale in the direction of mean flame propagation to the flame thickness. This aspect dominates over the higher turbulence intensity experienced by the $S_L/u_{\tau_{\mathrm{NR}}} = 0.4$ V-flame case away from the wall in comparison to that in the $S_L/u_{\tau_{\mathrm{NR}}} = 0.7$ V-flame case, which is responsible for the smaller value of S_T/S_L in the $S_L/u_{\tau_{\mathrm{NR}}} = 0.4$ V-flame case. Thus, the V-flame case for $S_L/u_{\tau_{\mathrm{NR}}} = 0.4$ exhibits a smaller flame angle than the V-flame case with $S_L/u_{\tau_{\mathrm{NR}}} = 0.7$.

The behavior of S_T/S_L and A_T/A_p in time for the planar flame HOI configuration is presented in Fig. 8, which shows that the case with $S_L/u_{\tau_{\mathrm{NR}}} = 0.4$ tends to have marginally higher maximum S_T/S_L and A_T/A_p values and tends to move faster in nondimensional time t/t_f when compared with the case with $S_L/u_{\tau_{\mathrm{NR}}} = 0.7$. Furthermore, the FWI occurs at a smaller value of t/t_f for $S_L/u_{\tau_{\mathrm{NR}}} = 0.4$. The main reason for the difference of S_T/S_L between the V-flame and the planar flame HOI configuration is due to the flame orientation with respect to the streamwise component of velocity. In the unsteady planar flame cases, the mean direction of flame propagation aligns with the wall-normal direction. The chemical time $t_f = \delta_{\mathrm{th}}/S_L$ and Karlovitz number Ka assume greater values in the $S_L/u_{\tau_{\mathrm{NR}}} = 0.4$ case than in the $S_L/u_{\tau_{\mathrm{NR}}} = 0.7$ case. This suggests that in addition to experiencing a higher ratio of the root-mean-square turbulence velocity to the unstretched laminar burning velocity, the flame is wrinkled by a comparative longer period of time in the $S_L/u_{\tau_{\mathrm{NR}}} = 0.4$ planar flame case than in the $S_L/u_{\tau_{\mathrm{NR}}} = 0.7$ planar flame case, which eclipses the effects of smaller integral length scale to flame thickness ratio in the $S_L/u_{\tau_{\mathrm{NR}}} = 0.4$ case. This means that the statistically planar flame in the $S_L/u_{\tau_{\mathrm{NR}}} = 0.4$ case is expected to be more wrinkled and its flame brush is expected to be thicker than that in the statistically planar $S_L/u_{\tau_{\mathrm{NR}}} = 0.7$ case. This can be substantiated by the variation of A_T/A_p as shown in Fig. 8. Thus, the FWI is expected to occur at smaller values of t/t_f in the statistically planar $S_L/u_{\tau_{\mathrm{NR}}} = 0.4$ case than in the corresponding $S_L/u_{\tau_{\mathrm{NR}}} = 0.7$ case.

The heat flux normalized in terms of chemical units is defined as $\Phi_w = |q_w|/[\rho_R S_L c_{p_R}(T_{\mathrm{ad}} - T_R)]$, where $q_w = -\lambda \partial \hat{T}/\partial y|_w$ is the dimensional wall heat flux, λ is the thermal conductivity

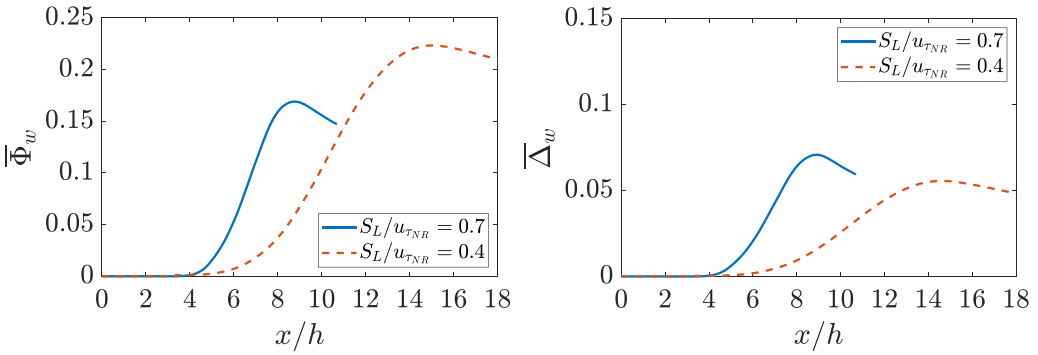

FIG. 9. The behavior of mean wall heat flux normalized in terms of chemical units, $\overline{\Phi}_w$, (left) and mean wall heat flux normalized in terms of wall units, $\overline{\Delta}_w$ (right) along the bottom wall in the axial direction for the V-flame cases with $S_L/u_{\tau_{\mathrm{NR}}} = 0.7$ and 0.4.

of the reacting gases, and c_{p_R} is the specific heat capacity of the reactants, while the heat flux normalized in terms of wall units is defined as $\Delta_w = |q_w|/[\rho_R \overline{u}_\tau c_{p_R}(T_{\mathrm{ad}} - T_R)]$. Figure 9 shows the mean normalized wall heat flux, where the heat flux is normalized in terms of chemical units, $\overline{\Phi}_w$, as well as the wall units, $\overline{\Delta}_w$. Both definitions of the mean wall heat flux are plotted along the length of the bottom wall of the channel in the case of the V-flame simulations in Fig. 9. In both definitions, the values of wall heat flux increase with streamwise distance in the case of V-flame OWI as the flame interacts with the wall and attains a maximum value at $x/h \approx 8$ for $S_L/u_{\tau_{\mathrm{NR}}} = 0.7$ and $x/h \approx 14$ for $S_L/u_{\tau_{\mathrm{NR}}} = 0.4$ before decreasing downstream of this location due to the thickening of the thermal boundary layer.

Note that in Fig. 9 the maximum $\overline{\Phi}_w$ and $\overline{\Delta}_w$ for the two cases are significantly different and the $S_L/u_{\tau_{\mathrm{NR}}} = 0.4$ case has the highest overall value for $\overline{\Phi}_w$ when compared with the $S_L/u_{\tau_{\mathrm{NR}}} = 0.7$ case. Whereas when the wall units are used to normalize the wall heat flux (i.e., $\overline{\Delta}_w$ in Fig. 9), the trends are reversed and the $S_L/u_{\tau_{\mathrm{NR}}} = 0.7$ case has the highest wall heat flux when compared with the $S_L/u_{\tau_{\mathrm{NR}}} = 0.4$ case. The temporal evolution of $\overline{\Phi}_w$ and $\overline{\Delta}_w$ in the case of planar flame HOI cases are presented in Fig. 10, which shows that $\overline{\Phi}_w$ and $\overline{\Delta}_w$ increase with time as the flame interacts with the wall and attain a maximum value at $t/t_f \approx 14.7$ for $S_L/u_{\tau_{\mathrm{NR}}} = 0.7$ and $t/t_f \approx 8$ for $S_L/u_{\tau_{\mathrm{NR}}} = 0.4$ cases subsequent to flame quenching. The peak value of $\overline{\Phi}_w$ in the statistically

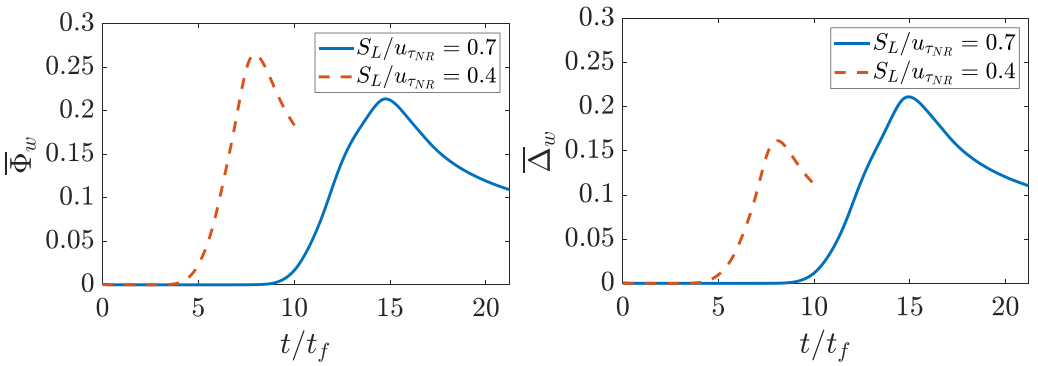

FIG. 10. Temporal evolution of mean wall heat flux normalized in terms of chemical units, $\overline{\Phi}_w$, (left) and mean wall heat flux normalized in terms of wall units, $\overline{\Delta}_w$ (right) for planar flame HOI cases with $S_L/u_{\tau_{\mathrm{NR}}} = 0.7$ and 0.4.

planar flame HOI case with $S_L/u_{\tau_{NR}} = 0.4$ is found to be greater than in the statistically planar $S_L/u_{\tau_{NR}} = 0.7$ flame case, while the opposite trend is observed for $\overline{\Delta}_w$ in these cases.

The discrepancy between the two normalizations in these cases can be explained by scaling arguments. The laminar burning velocity for the thermochemistry in the $S_L/u_{\tau_{NR}} = 0.4$ case is 1.75 times smaller than that in the $S_L/u_{\tau_{NR}} = 0.7$ case but $\overline{\Phi}_w$ in the $S_L/u_{\tau_{NR}} = 0.4$ planar flame case is not 1.75 times greater than that in the $S_L/u_{\tau_{NR}} = 0.7$ planar flame case. This suggests that the peak value of the mean wall heat flux magnitude in the $S_L/u_{\tau_{NR}} = 0.4$ flame cases is actually smaller than that in the $S_L/u_{\tau_{NR}} = 0.7$ flame cases. The minimum quenching distance y_Q (quantified by the wall-normal distance of the $T = 0.75$ isosurface) normalized by the Zeldovich flame thickness δ_Z for the cases considered are 1.82 and 1.71 for the V-flame and the statistically planar HOI cases, respectively, with $S_L/u_{\tau_{NR}} = 0.7$, while these values are 1.77 and 1.79 for the V-flame and the statistically planar HOI cases, respectively, with $S_L/u_{\tau_{NR}} = 0.4$. Note that y_Q scales with $\sim D_c/S_L$ for all cases. As δ_Z is greater in the $S_L/u_{\tau_{NR}} = 0.4$ case when compared with the $S_L/u_{\tau_{NR}} = 0.7$ case, the flame quenches farther away from the wall in the $S_L/u_{\tau_{NR}} = 0.4$ case which acts to yield a smaller maximum value of $|q_{w_{max}}| \sim \rho_R C_{PR} T_R D_c \Gamma / y_Q$ in this case for both V-flame and statistically planar flame configurations. Using $\overline{u}_\tau \sim \nu/y_v$ (with ν and y_v being the kinematic viscosity and viscous sub-layer thickness, respectively), the mean heat flux normalized by wall units can be scaled as: $\overline{\Delta}_w \sim y_v/y_Q$, which, in turn, can be scaled with $S_L/\overline{u}_\tau$ as y_Q scales with D_c/S_L and the Schmidt number (i.e., $Sc = \nu/D_c$) remains of the order of unity. This implies that for FWI within turbulent boundary layers the mean wall heat flux normalized by the wall units increases with $S_L/u_{\tau_{NR}}$.

To investigate the variation of turbulence-related quantities in wall units, the mean values of the wall shear stress, $\overline{\tau}_w$, and the mean value of the wall friction velocity, $\overline{u}_\tau = \sqrt{|\overline{\tau}_w|/\overline{\rho}_w}$, are presented in Fig. 11 at top and bottom walls for the V-flame cases. Note that these values are normalized by the corresponding nonreacting values so that the influence of the different $S_L/u_{\tau_{NR}}$ conditions on $\overline{\tau}_w$ and $\overline{u}_\tau$ can be identified. Figure 11 shows that the distributions of $\overline{\tau}_w$ and $\overline{u}_\tau$ are affected by the changes in $S_L/u_{\tau_{NR}}$. The qualitative behavior of $\overline{\tau}_w$ and $\overline{u}_\tau$ is almost identical for the top wall under different $S_L/u_{\tau_{NR}}$ conditions, but the magnitudes are different due to the difference in $S_L/u_{\tau_{NR}}$. In the case of $S_L/u_{\tau_{NR}} = 0.7$, higher values of $\overline{\tau}_w$ and $\overline{u}_\tau$ are observed on the top wall when compared with those obtained in the $S_L/u_{\tau_{NR}} = 0.4$ case downstream of the flame holder. In the V-flame cases, an increase in $\overline{\tau}_w$ and $\overline{u}_\tau$ is obtained due to the flow acceleration in the streamwise direction caused by the thermal expansion effects within the turbulent boundary layer for both $S_L/u_{\tau_{NR}}$ ratios. For the V-flame case with $S_L/u_{\tau_{NR}} = 0.7$, a localized drop in values of $\overline{\tau}_w$ and $\overline{u}_\tau$ can be seen in the region of FWI (x/h between 6.5 to 9). By contrast, in the case of V-flame with $S_L/u_{\tau_{NR}} = 0.4$, the values of $\overline{\tau}_w$ and $\overline{u}_\tau$ are not affected much until after FWI and no significant increase or decrease in the values of $\overline{\tau}_w$ and $\overline{u}_\tau$ is observed during FWI. In both cases, an increase in $\overline{\tau}_w$ and $\overline{u}_\tau$ at $x/h \approx 1$ is seen due to the proximity of the flame holder to the bottom wall, which leads to flow acceleration further upstream when compared with the top wall. It should be noted that the increase in the values of $\overline{\tau}_w$ and $\overline{u}_\tau$ after FWI in both V-flame cases is a result of flow acceleration in the streamwise direction caused by the thermal expansion effects due to the flame. The temporal variation of $\overline{\tau}_w$ and $\overline{u}_\tau$ in the planar flame HOI cases is presented in Fig. 12. In this case, the overall variation of $\overline{\tau}_w$ and $\overline{u}_\tau$ is similar between the two $S_L/u_{\tau_{NR}}$ ratios, but slightly lower values of $\overline{\tau}_w$ and $\overline{u}_\tau$ are obtained during FWI for $S_L/u_{\tau_{NR}} = 0.4$. As explained earlier in the paper, the planar flame HOI case with $S_L/u_{\tau_{NR}} = 0.4$ interacts with the wall at smaller values of $t_f = \delta_{th}/S_L$ when compared with the $S_L/u_{\tau_{NR}} = 0.7$ case. This has an effect on how the velocity gradients evolve as a function of t/t_f within the turbulent boundary layer and as a consequence small variations in $\overline{\tau}_w$ and $\overline{u}_\tau$ are observed between the two $S_L/u_{\tau_{NR}}$ ratios for planar flame HOI cases.

Figure 13 shows the variation of the Favre mean nondimensional velocity, $u^+ = \widetilde{u}/\overline{u}_\tau$, against y^+ from the bottom wall up to the centerline of the channel in the V-flame cases at different locations downstream of the flame holder within the region of flame-wall interaction. Note that for the evaluation of u^+ and y^+ in Fig. 13, local values of $\overline{u}_\tau$ are used. The standard trend for $u^+ = y^+$ is obeyed within the viscous sublayer (i.e., $y^+ \leqslant 5$) in the V-flame cases at both values of $S_L/u_{\tau_{NR}}$ considered. In the region $y^+ > 20$, significant deviations from the log-law and the corresponding

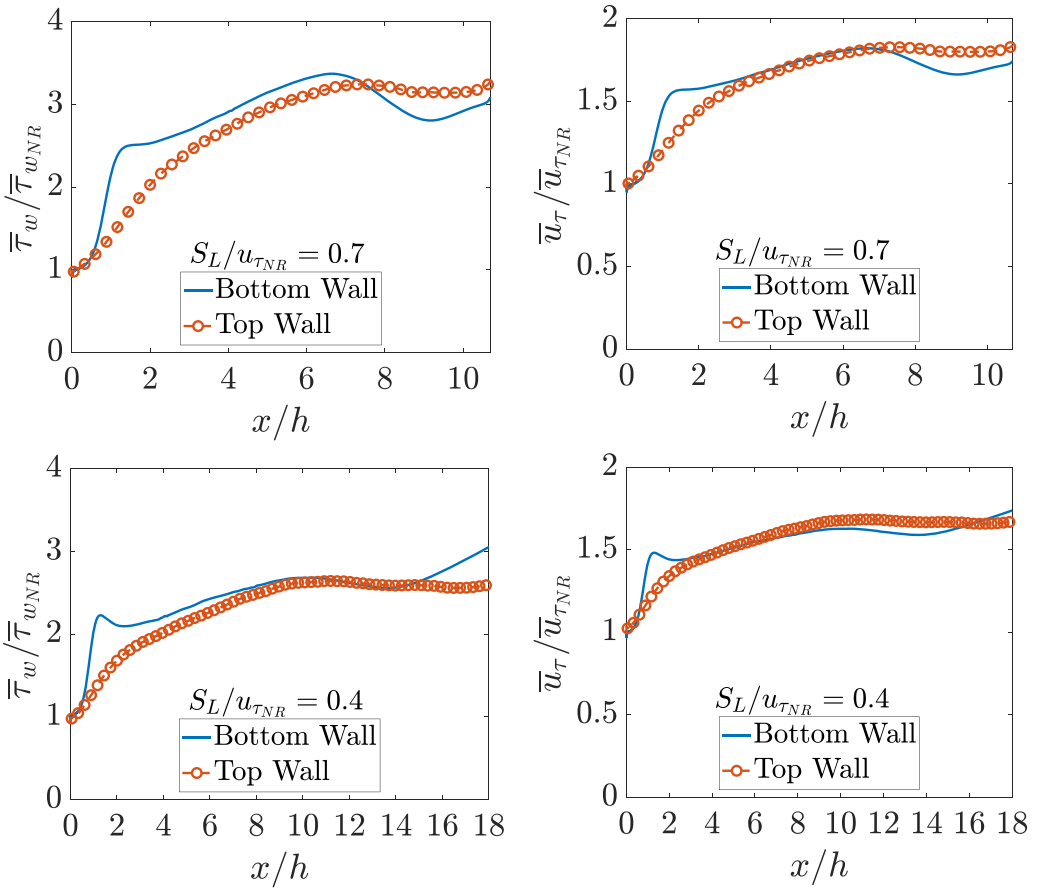

FIG. 11. Profiles for $\overline{\tau}_w$ and $\overline{u}_\tau$ along the top and bottom walls in the axial direction in the V-flame cases with $S_L/u_{\tau_{\mathrm{NR}}} = 0.7$ and 0.4.

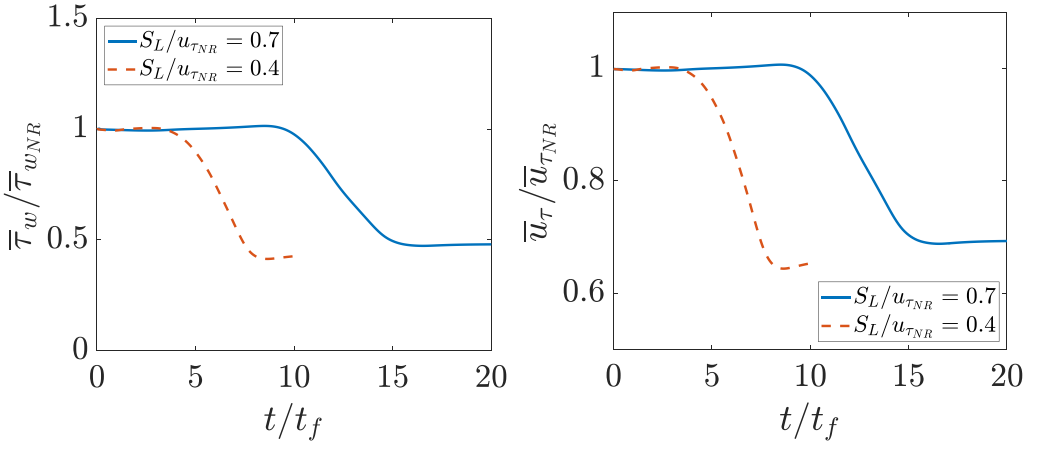

FIG. 12. Temporal evolution of $\overline{\tau}_w$ and $\overline{u}_\tau$ at the wall for the planar flame HOI cases with $S_L/u_{\tau_{\mathrm{NR}}} = 0.7$ and 0.4.

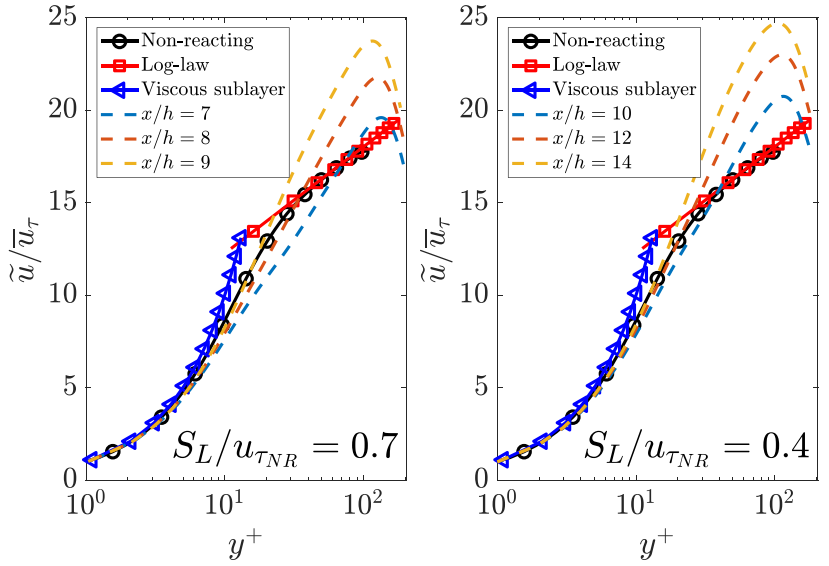

FIG. 13. Variation of $u^+ = \widetilde{u}/\overline{u}_\tau$ against nondimensional distance to the bottom wall, y^+, for the V-flame cases with $S_L/u_{\tau_{\mathrm{NR}}} = 0.7$ and 0.4.

nonreacting channel flow can be seen for $S_L/u_{\tau_{\mathrm{NR}}} = 0.7$ and $S_L/u_{\tau_{\mathrm{NR}}} = 0.4$ cases. This deviation from log-law in the case of flame-wall interaction increases as the flame quenching progresses. The variation of u^+ against y^+ at different times for the planar flame HOI cases is shown in Fig. 14. As with the V-flame cases, a good collapse of data in the viscous sublayer can be seen at all time instants for the reacting and nonreacting turbulent boundary layers, where the nonreacting data corresponds to the nonreacting turbulent channel flow. A disparity between the reacting and nonreacting data,

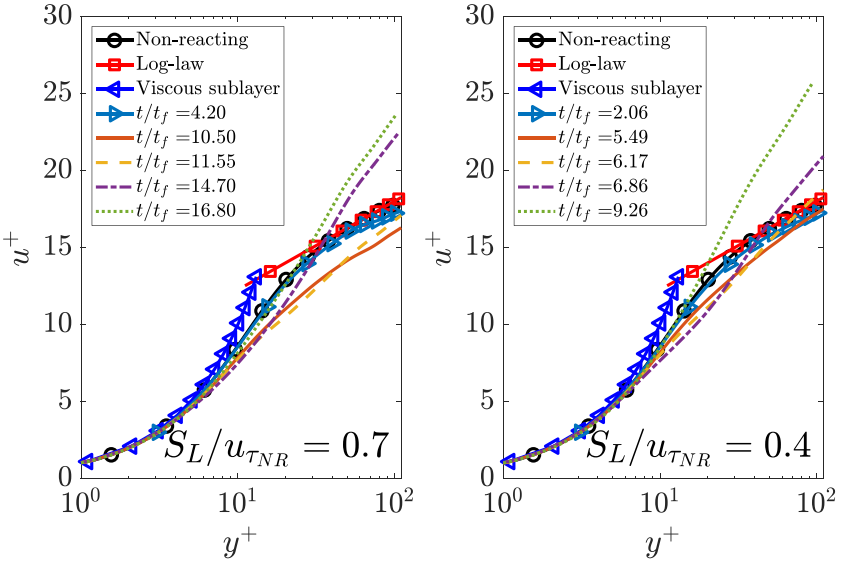

FIG. 14. Variation of $u^+ = \widetilde{u}/\overline{u}_\tau$ against nondimensional distance to the wall, y^+, for the planar flame HOI cases with $S_L/u_{\tau_{\mathrm{NR}}} = 0.7$ and 0.4.

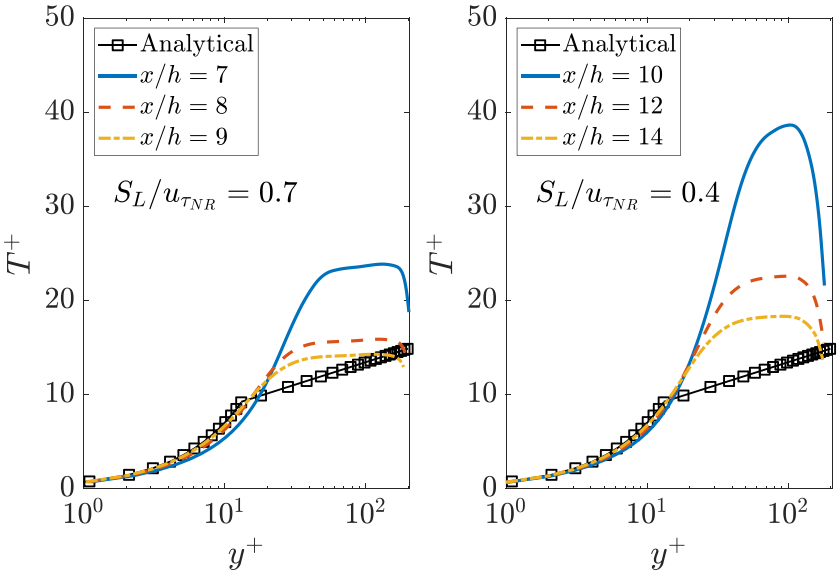

FIG. 15. Variation of T^+ against non-dimensional distance to the bottom wall, y^+, for the V-flame cases with $S_L/u_{\tau_{\mathrm{NR}}} = 0.7$ and 0.4.

including the conventional log-law, can be observed outside the viscous sublayer region for all time instants. This deviation from log-law in the case of flame-wall interaction increases as the flame quenching progresses in both configurations. It has been explained by Ghai *et al.* [11] and Ahmed *et al.* [35] that the underlying assumptions behind the log-law (i.e., validity of Boussinesq's hypothesis and the local equilibrium between turbulent kinetic energy production and viscous dissipation rate) are not maintained during flame-wall interaction within turbulent boundary layer. These results are also consistent with the recent experimental findings of Zentgraf *et al.* [34].

The nondimensional temperature using wall units, $T^+ = (T_w - \widetilde{\hat{T}})\overline{\rho}_w c_{p_w} \overline{u}_\tau / \overline{q}_w$, against y^+ is presented in Fig. 15 for different locations downstream of the flame holder for the V-flame cases. The results from both V-flame cases are compared with the analytical expression for T^+ proposed by Kays and Crawford [40] for flows without reaction in fully developed turbulence and turbulent heat flux based on the Reynolds analogy. The analytical expression proposed by Kays and Crawford [40] reads $T^+ = (\mathrm{Pr}_t/\kappa)\ln(y^+/y^+_{\mathrm{crit}}) + y^+_{\mathrm{crit}}\mathrm{Pr}$, where Pr_t is the turbulent Prandtl number, κ is the von Karman constant, and y^+_{crit} is the thermal sublayer thickness in wall units. This expression is valid for $y^+ > 30$ and suggested values for the constants are $\mathrm{Pr}_t = 0.85$, $\kappa = 0.41$, and $y^+_{\mathrm{crit}} = 13.2$ [40]. In the case of the V-flame simulations, the influence of the flame holder on the T^+ profile can be seen at $y^+ \approx 55$ in Fig. 15. The T^+ profiles are in reasonable agreement with the analytical profile in the viscous sublayer region for the V-flame cases, beyond which a significant deviation occurs in the log-layer region for all the sampling locations which is a consequence of $\overline{\Delta}_w$ variation and in the V-flame case with $S_L/u_{\tau_{\mathrm{NR}}} = 0.4$ higher T^+ values are observed due to lower values of $\overline{\Delta}_w$, as shown in Fig. 9, in this case when compared with the $S_L/u_{\tau_{\mathrm{NR}}} = 0.7$ case. Figure 16 shows the variation of T^+ with y^+ in the case of planar flame HOI cases at different times and similar trends as for the V-flame cases are observed. It can be noticed in Fig. 16 that for both $S_L/u_{\tau_{\mathrm{NR}}}$ ratios the analytical profile does not match in the log-layer region. Furthermore, similar to the V-flame $S_L/u_{\tau_{\mathrm{NR}}} = 0.4$ case, the values for T^+ are much higher in the case of $S_L/u_{\tau_{\mathrm{NR}}} = 0.4$ due to the lower values of $\overline{\Delta}_w$ as shown in Fig. 10. It is worth noting that the log-law for temperature is derived based on the assumption of the log-law for the mean streamwise velocity component, but this assumption is rendered invalid during FWI, as shown in Figs. 13 and 14, so it is perhaps not surprising that the log-law for temperature does not remain valid for the premixed cases considered here.

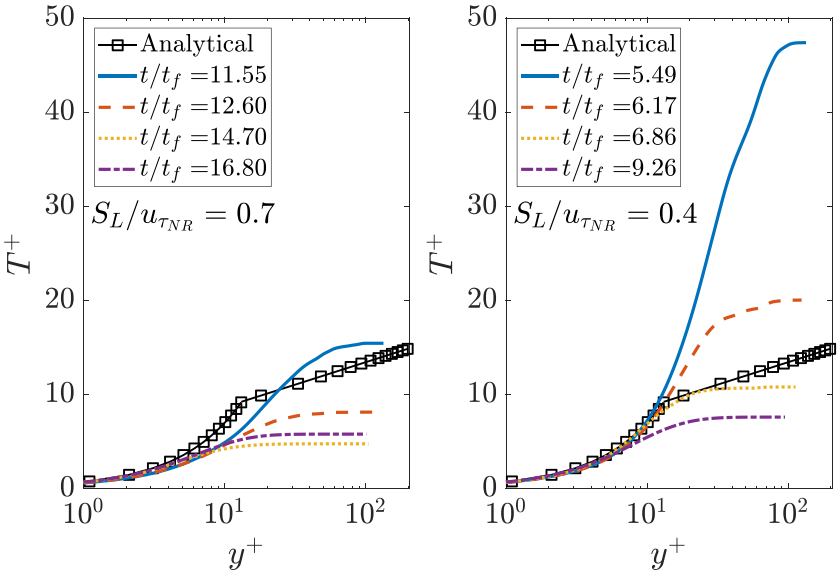

FIG. 16. Variation of T^+ against non-dimensional distance to the wall, y^+, for the planar flame HOI cases with $S_L/u_{\tau_{\mathrm{NR}}} = 0.7$ and 0.4.

IV. CONCLUSIONS

DNS of a V-flame in a fully developed turbulent channel flow at $\mathrm{Re}_\tau = 110$ representative of an OWI and a HOI of a planar flame in a fully developed turbulent boundary layer at $\mathrm{Re}_\tau = 110$ have been performed under isothermal inert wall boundary conditions for two different laminar burning velocity to nonreacting flow wall friction velocity ratios, $S_L/u_{\tau_{\mathrm{NR}}} = 0.4$ and 0.7. The following observations are made in this paper:

(1) It is shown that the flow configuration plays a role in the behavior of turbulent burning velocity, wall heat flux, wall shear stress, and wall friction velocity for different values of $S_L/u_{\tau_{\mathrm{NR}}}$.

(2) In the case of the V-flame with $S_L/u_{\tau_{\mathrm{NR}}} = 0.4$, a smaller flame angle is obtained when compared with that of the V-flame with $S_L/u_{\tau_{\mathrm{NR}}} = 0.7$. This is a consequence of the differences in the turbulent burning velocities between the two V-flame cases, where the case with $S_L/u_{\tau_{\mathrm{NR}}} = 0.4$ has a lower turbulent burning velocity when compared with that of the case with $S_L/u_{\tau_{\mathrm{NR}}} = 0.7$.

(3) The planar flame HOI case with $S_L/u_{\tau_{\mathrm{NR}}} = 0.4$ has a marginally higher S_T/S_L when compared with the planar flame HOI with $S_L/u_{\tau_{\mathrm{NR}}} = 0.7$.

(4) The flame orientations with respect to the streamwise velocity component and wall-normal direction along with thermochemistry affect the variation of S_T/S_L in response to the variations of $S_L/u_{\tau_{\mathrm{NR}}}$ and flame configuration.

(5) The behaviors of nondimensional streamwise velocity u^+ and nondimensional temperature using wall units T^+ for different $S_L/u_{\tau_{\mathrm{NR}}}$ ratios show that the standard log-law profiles in the case of u^+ and T^+ are not valid for the two configurations and the two $S_L/u_{\tau_{\mathrm{NR}}}$ ratios considered.

These variations and similarities have implications on the mean wall heat flux, wall shear stresses, and wall friction velocity, which need to be accounted for to improve the modeling of premixed FWI within turbulent boundary layers.

ACKNOWLEDGMENTS

Financial support was provided by EPSRC (EP/V003534/1). The computational support was provided by EPSRC (EP/R029369/1), ARCHER2 Pioneer project (e691), SuperMUC-NG (pn69ga, pn34xu), and ROCKET-HPC at Newcastle University.

[1] T. J. Poinsot and D. Veynante, *Theoretical and Numerical Combustion*, 2nd ed. (R. T. Edwards, Inc, Philadelphia, USA, 2005).
[2] T. M. Alshaalan and C. J. Rutland, Turbulence, scalar transport, and reaction rates in flame-wall interaction, Symp. (Int.) Combust. **27**, 793 (1998).
[3] G. Bruneaux, K. Akselvoll, T. J. Poinsot, and J. H. Ferziger, Flame-wall interaction simulation in a turbulent channel flow, Combust. Flame **107**, 27 (1996).
[4] G. Bruneaux, T. J. Poinsot, and J. H. Ferziger, Premixed flame-wall interaction in a turbulent channel flow: Budget for the flame surface density evolution equation and modelling, J. Fluid Mech. **349**, 191 (1997).
[5] A. Gruber, R. Sankaran, E. R. Hawkes, and J. H. Chen, Turbulent flame-wall interaction: A direct numerical simulation study, J. Fluid Mech. **658**, 5 (2010).
[6] U. Ahmed, N. Chakraborty, and M. Klein, Scalar gradient and strain rate statistics in oblique premixed flame-wall interaction within turbulent channel flows, Flow, Turbul. Combust. **106**, 701 (2021).
[7] B. Jiang, D. Brouzet, M. Talei, R. L. Gordon, Q. Cazeres, and B. Cuenot, Turbulent flame-wall interactions for flames diluted by hot combustion products, Combust. Flame **230**, 111432 (2021).
[8] R. Kai, A. L. Pillai, U. Ahmed, N. Chakraborty, and R. Kurose, Analysis of the evolution of the surface density function during premixed V-Shaped flame–wall interaction in a turbulent channel flow at $\mathrm{Re}\tau = 395$, Combust. Sci. Technol. **00**, 1 (2022).
[9] U. Ahmed, N. Chakraborty, and M. Klein, Influence of flow configuration and thermal wall boundary conditions on turbulence during premixed flame-wall interaction within low Reynolds number boundary layers, Flow Turbul. Combust. **111**, 825 (2023).
[10] S. K. Ghai, N. Chakraborty, U. Ahmed, and M. Klein, Enstrophy evolution during head-on wall interaction of premixed flames within turbulent boundary layers, Phys. Fluids **34**, 075124 (2022).
[11] S. Ghai, U. Ahmed, M. Klein, and N. Chakraborty, Turbulent kinetic energy evolution in turbulent boundary layers during head-on interaction of premixed flames with inert walls for different thermal boundary conditions, Proc. Combust. Inst. **39**, 2169 (2023).
[12] S. Ghai, U. Ahmed, and N. Chakraborty, Effects of fuel lewis number on wall heat transfer during oblique flame-wall interaction of premixed flames within turbulent boundary layers, Flow Turbul. Combust. **111**, 867 (2023).
[13] M. Steinhausen, T. Zirwes, F. Ferraro, A. Scholtissek, H. Bockhorn, and C. Hasse, Flame-vortex interaction during turbulent side-wall quenching and its implications for flamelet manifolds, Proc. Combust. Inst. **39**, 2149 (2023).
[14] U. Ahmed, N. Chakraborty, and M. Klein, Influence of thermal wall boundary condition on scalar statistics during flame-wall interaction of premixed combustion in turbulent boundary layers, Int. J. Heat Fluid Flow **92**, 108881 (2021).
[15] S. Ghai, U. Ahmed, M. Klein, and N. Chakraborty, Energy integral equation for premixed flame-wall interaction in turbulent boundary layers and its application to turbulent burning velocity and wall flux evaluations, Int. J. Heat Mass Transf. **196**, 123230 (2022).
[16] D. Kaddar, M. Steinhausen, T. Zirwes, H. Bockhorn, C. Hasse, and F. Ferraro, Combined effects of heat loss and curvature on turbulent flame-wall interaction in a premixed dimethyl ether/air flame, Proc. Combust. Inst. **39**, 2199 (2023).
[17] N. Peters, *Turbulent Combustion* (Cambridge University Press, Cambridge, 2000).
[18] K. Jenkins and R. Cant, Direct numerical simulation of turbulent flame kernels, in *Recent Advances in DNS and LES: Proceedings of the Second AFOSR Conference, Rutgers - The State University of New Jersey, New Brunswick, USA*, edited by D. Knight and L. Sakell (Kluwer, Dordrecht, 1999), pp. 191–202.
[19] J. Lai and N. Chakraborty, A Priori direct numerical simulation modeling of scalar dissipation rate transport in head-on quenching of turbulent premixed flames, Combust. Sci. Technol. **188**, 1440 (2016).
[20] P. Zhao, L. Wang, and N. Chakraborty, Analysis of the flame–wall interaction in premixed turbulent combustion, J. Fluid Mech. **848**, 193 (2018).
[21] P. Zhao, L. Wang, and N. Chakraborty, Strain rate and flame orientation statistics in the near-wall region for turbulent flame-wall interaction, Combust. Theory Model. **22**, 921 (2018).

[22] A. Gruber, J. H. Chen, D. Valiev, and C. K. Law, Direct numerical simulation of premixed flame boundary layer flashback in turbulent channel flow, J. Fluid Mech. **709**, 516 (2012).
[23] J. Lai, N. Chakraborty, P. Zhao, and L. Wang, Heat flux and flow topology statistics in oblique and head-on quenching of turbulent premixed flames by isothermal inert walls, Combust. Sci. Technol. **191**, 353 (2019).
[24] J. Lai, U. Ahmed, M. Klein, and N. Chakraborty, A comparison between head-on quenching of stoichiometric methane-air and hydrogen-air premixed flames using Direct Numerical Simulations, Int. J. Heat Fluid Flow **93**, 108896 (2022).
[25] D. Zhao, F. E. Zhang, C. Hernández Pérez, H. G. Im, and L. Wang, Near wall effects on the premixed head-on hydrogen/air flame, Combust. Flame **244**, 112267 (2022).
[26] D. Zhao, F. E. Zhang, C. Hernández Pérez, H. G. Im, and L. Wang, Turbulent premixed hydrogen/air flame-wall interaction with heterogeneous surface reactions, Proc. Combust. Inst. **39**, 2189 (2023).
[27] S. Vosen, R. Greif, and C. K. Westbrook, Unsteady heat transfer during laminar flame quenching, Symposium (International) on Combustion **20**, 75 (1985).
[28] J. Jarosinski, A survey of recent studies on flame extinction, Prog. Energy Combust. Sci. **12**, 81 (1986).
[29] C. Jainski, M. Rißmann, B. Böhm, and A. Dreizler, Experimental investigation of flame surface density and mean reaction rate during flame-wall interaction, Proc. Combust. Inst. **36**, 1827 (2017).
[30] M. D. Smooke and V. Giovangigli, *Premixed and Nonpremixed Test Problem Results* (Springer, Berlin, 1991), pp. 29–47.
[31] T. D. Dunstan, N. Swaminathan, K. N. C. Bray, and R. S. Cant, Geometrical properties and turbulent flame speed measurements in stationary premixed V-flames using direct numerical simulation, Flow Turbul. Combust. **87**, 237 (2010).
[32] U. Ahmed, D. D. Apsley, T. Stallard, P. K. Stansby, and I. Afgan, Turbulent length scales and budgets of Reynolds stress-transport for open-channel flows; friction Reynolds numbers $\mathrm{Re}\tau = 150$, 400, and 1020, J. Hydraul. Res. **59**, 36 (2021).
[33] U. Ahmed, N. Chakraborty, and M. Klein, Assessment of Bray Moss Libby formulation for premixed flame-wall interaction within turbulent boundary layers: Influence of flow configuration, Combust. Flame **233**, 111575 (2021).
[34] F. Zentgraf, P. Johe, A. Nicolas, R. S. Barlow, B. Böhm, B. Peterson, and A. Dreizler, On the evolution of turbulent boundary layers during flame–wall interaction investigated by highly resolved laser diagnostics, Combust. Flame **261**, 113276 (2024).
[35] U. Ahmed, S. K. Ghai, and N. Chakraborty, Assessment of laws of the wall during flame–wall interaction of premixed flames within turbulent boundary layers, Flow Turbul. Combust. **112**, 1161 (2024).
[36] U. Ahmed, S. K. Ghai, and N. Chakraborty, Relations between Reynolds stresses and their dissipation rates during premixed flame-wall interaction within turbulent boundary layers, Phys. Fluids **36**, 045120 (2024).
[37] C. Jainski, M. Rißmann, S. Jakirlic, B. Böhm, and A. Dreizler, Quenching of premixed flames at cold walls: Effects on the local flow field, Flow Turbul. Combust. **100**, 177 (2018).
[38] A. R. Varma, U. Ahmed, and N. Chakraborty, Effects of body forces on vorticity and enstrophy evolutions in turbulent premixed flames, Phys. Fluids **33**, 035102 (2021).
[39] W. Song, F. Hernandez-Perez, E. Tingas, and H. Im, Statistics of local and global flame speed and structure for highly turbulent H_2/air premixed flames, Combust. Flame **232**, 111523 (2021).
[40] W. M. Kays and M. E. Crawford, *Convective Heat and Mass Transfer*, 3rd ed. (McGraw-Hill, New York, 1993).